ORIGINAL ARTICLE

Nitrogen-mediated metabolic patterns of susceptibility to *Botrytis cinerea* infection in tomato (*Solanum lycopersicum*) stems

Nathalie Lacrampe[1,2] · Sophie Colombié[3] · Doriane Dumont[1] · Philippe Nicot[4] · François Lecompte[1] · Raphaël Lugan[2]

Abstract

Main conclusion Severe N stress allows an accumulation of C-based compounds but impedes that of N-based compounds required to lower the susceptibility of tomato stem to *Botrytis cinerea*.

Abstract *Botrytis cinerea*, a necrotrophic filamentous fungus, forms potentially lethal lesions on the stems of infected plants. Contrasted levels of susceptibility to *B. cinerea* were obtained in a tomato cultivar grown on a range of nitrate concentration: low N supply resulted in high susceptibility while high N supply conferred a strong resistance. Metabolic deviations and physiological traits resulting from both infection and nitrogen limitation were investigated in the symptomless stem tissue surrounding the necrotic lesion. Prior to infection, nitrogen-deficient plants showed reduced levels of nitrogen-based compounds such as amino acids, proteins, and glutathione and elevated levels of carbon-based and defence compounds such as α-tomatine and chlorogenic acid. After *B. cinerea* inoculation, all plants displayed a few common responses, mainly alanine accumulation and galactinol depletion. The metabolome of resistant plants grown under high N supply showed no significant change after inoculation. On the contrary, the metabolome of susceptible plants grown under low N supply showed massive metabolic adjustments, including changes in central metabolism around glutamate and respiratory pathways, suggesting active resource mobilization and production of energy and reducing power. Redox and defence metabolisms were also stimulated by the infection in plants grown under low N supply; glutathione and chlorogenic acid accumulated, as well as metabolites with more controversial defensive roles, such as polyamines, GABA, branched-chain amino acids and phytosterols. Taken together, the results showed that nitrogen deficiency, although leading to an increase in secondary metabolites even before the pathogen attack, must have compromised the constitutive levels of defence proteins and delayed or attenuated the induced responses. The involvement of galactinol, alanine, cycloartenol and citramalate in the tomato stem response to *B. cinerea* is reported here for the first time.

Keywords *Botrytis cinerea* · Nitrate · Plant−pathogen interaction · Defence metabolism · Plant metabolomicss

✉ Raphaël Lugan
raphael.lugan@univ-avignon.fr

Nathalie Lacrampe
nathalie.lacrampe@alumni.univ-avignon.fr

Sophie Colombié
sophie.colombie@inrae.fr

Doriane Dumont
doriane.dumont@inrae.fr

Philippe Nicot
philippe.nicot@inrae.fr

François Lecompte
francois.lecompte.2@inrae.fr

[1] PSH Unit, INRAE, 84914 Avignon, France

[2] UMR Qualisud, Avignon Université, 84916 Avignon, France

[3] UMR 1332 BFP, INRAE, Univ Bordeaux, 33883 Villenave d'Ornon, France

[4] Plant Pathology Unit, INRAE, 84140 Montfavet, France

Introduction

Botrytis cinerea (perfect stage: *Botryotinia fuckeliana*) is a filamentous fungus able to infect over 200 dicot hosts. In tomato, conidia that germinate on wilted tissues or leaf removal wounds may generate lesions potentially lethal to the plant when they spread to the stem (Holz et al. 2007). It is usually considered as a necrotroph, which employs a large arsenal of virulence factors (toxic compounds, reactive oxygen species (ROS), cell wall degrading enzymes, proteases and necrosis-inducing proteins) that lead to tissue decay and rapid fungal growth (Choquer et al. 2007). The screening of Arabidopsis mutants infected by *B. cinerea* revealed the critical role of cell death in fungal propagation (Van Baarlen et al. 2007) and highlighted the role of plant tissues surrounding the infection site in the control of pathogen-induced senescence.

Plant defence is partly passive and constitutive but, presumably because of its energetic cost, is mainly triggered upon pathogen detection (Heil and Baldwin 2002). Constitutive defences include phytoanticipins, antimicrobial compounds preformed or released from constitutive precursors after pathogen invasion, such as α-tomatine, a steroidal glycoalkaloid found in most organs in the *Solanaceae* family (Friedman 2002). The role of ROS in necrotrophic interactions is ambivalent, and the timing and intensity of their production are critical (Asselbergh et al. 2007). On the one hand, they participate in host cell wall reinforcement and signal transduction pathways, as well as localized cell death at the site of infection, but on the other hand, several lines of evidence suggest that necrotrophic fungi produce ROS that contribute to programmed cell death and promote fungal propagation (Rossi et al. 2017).

Host defence activation following *B. cinerea* infection is accompanied by massive transcriptional reprogramming (Windram et al. 2012; De Cremer et al. 2013), notably causing changes in the expression of metabolism-associated genes, most commonly the repression of photosynthesis-associated genes and the activation of genes involved in defence secondary pathways, including phenolics, these responses being confirmed by direct measurements in tomato (Chen et al. 2021). Metabolomic studies are also in line with these findings (Camañes et al. 2015; Gao et al. 2021), highlighting the role of phenolic compounds following *B. cinerea* infection, notably the accumulation of hydroxycinnamic acids such as ferulic and caffeic acids, which are precursors of lignins and cross-linkers of cell wall polysaccharides. Regarding the adaptation of primary metabolism, there is a general acceptance that the role of primary metabolism is to fuel plant defence by providing energy, reducing equivalents and basic C and N skeletons for phytoalexins and defence-related proteins (Bolton 2009). In source organs such as leaves, the decline in photosynthesis observed after infection by *B. cinerea* is likely to constrain these supplies, although, on the other hand, the depletion of photoassimilates does not favour the feeding of the pathogen. The portrait resulting from transcriptomic and metabolomic studies is also ambivalent. Microarray analysis on tomato leaves has shown the repression of genes involved in glycolysis and the oxidative pentose phosphate pathway (OPPP), as well as an upregulation of the genes involved in the TCA cycle (Camañes et al. 2015), while in contrast, genes involved in glycolysis, OPPP and TCA cycle were upregulated in lettuce leaves infected with *B. cinerea* (De Cremer et al. 2013). In healthy grape berries among a *Botrytis*-infected bunch, an increased content of several amino acids, including arginine, valine, leucine, isoleucine and threonine, contrasted with their depletion in tomato leaves following infection (Hong et al. 2012). These discrepancies may arise from the nature of the tissues observed but also from their metabolic status at the time of infection. Depending on the environment, in particular the combined levels of radiation, water and nutrient availability, the metabolic activity and the resulting concentrations of metabolic intermediates can vary to a large extent.

The influence of nitrogen on host-pathogen interactions has been observed for a very long time but is still poorly understood due to the number of phenomena involved and their complexity (Fagard et al. 2014). Nitrogen shapes the plant architecture and the microclimate around organs, influences host metabolism and defence, and is also a nutrient resource that may regulate pathogen virulence. Elevated N availability for the host plant favours the incidence and/or expansion of *B. cinerea* (Lecompte et al. 2013; Nicot et al. 2013; Soulie et al. 2020). Conversely, high N decreases disease severity in both tomato leaves and stems (Hoffland et al. 1999; Vega et al. 2015). A transcriptomic study conducted on Arabidopsis by Soulie et al. (2020) found no definitive explanation for the contrast in resistance to *B. cinerea* under low or high N nutrition regimes but reported infection-induced changes in the expression of several genes related to N transport and/or metabolism, regardless of the N status, with the notable exceptions of nitrate reductase 1 and asparagine synthase 1. Interestingly, some defence genes were more strongly expressed in plants grown under low N supply, suggesting a regulatory role of N nutrition on the defences going beyond the simple supply of substrates. The integration of defence and nitrogen nutrition mechanisms was also investigated with transcriptomic analyses of tomato shoots infected by *B. cinerea* (Vega et al. 2015). This work showed that plants well supplied with nitrogen and resistant to the pathogen overexpressed *NTR2*, a high-affinity NO_3^- transporter, as well as genes coding for defence proteins such as PADRE protein, chitinases and

secondary metabolic pathways enzymes such as homologues of CYP75B1 and CYP84A1 involved in flavonoid biosynthesis and lignin biosynthesis, respectively. Although transcriptomic variations do not fully correlate with proteomic variations (Feussner and Polle 2015; Stare et al. 2017), these results suggested that resistance was based on a proteome configuration depending on the plant nitrogen status.

The aim of our work was to study the metabolomic response to *B. cinerea* of symptomless tomato stem tissues adjacent to the lesion under five N supplies, ranging from a severe deficit (0.5 mM NO_3^-) to overfertilization (20 mM NO_3^-). A combination of untargeted and multitargeted metabolomics (Allwood et al. 2021) allowed us to explore key portions of the metabolome, including primary metabolites and some important defence metabolites in tomato. We first studied the impact of N supply on physiological traits and the metabolome. Then, we identified metabolic markers associated with infection by the fungus and discussed how these metabolic adjustments induced by N supply could favour resistance or susceptibility.

Materials and methods

Plant materials

Biological samples were obtained as previously described (Lacrampe et al. 2021). Briefly, tomato plants (*Solanum lycopersicum* CV "Clodano"; Syngenta, Wilmington, DE, USA) were grown in glasshouse from February to March 2018. Tomato seeds were sown and the seedlings were transferred 10 days after germination onto rock wool blocks. After three additional weeks, the plants (bearing three or four leaves) were placed on top of 2-L pots filled with a mixture (1:1 v/v) of vermiculite and pozzolana. From germination to the beginning of the nitrate treatment, the plants were fertigated twice a day with a standard commercial nutrient solution (Liquoplant Rose; Plantin, Courthézon, France). Seven weeks after germination, plants were fertigated for another four weeks, using a drip irrigation system (one dripper per pot) up to nine times a day depending on the climatic demand, with five nutrient solutions containing NO_3^- concentrations of 0.5, 2, 5, 10 and 20 mM. Thirty-five plants were used for each NO_3^- treatment, corresponding to seven batches of five biological replicates, sampled just before inoculation (0 days post-inoculation, dpi), and then 2, 4 and 7 dpi. Inoculations were carried out on the petiole stubs (5–7 mm long) that remained on the stems after the excision of the sixth leaf. The wounds received a 10-μL aliquot of either the spore suspension (*Botrytis*-inoculated plants) or sterile water (mock-inoculated plants). Two-cm long fragments of the symptomless stem were collected between the fifth and sixth internode. The collected samples were immediately frozen in liquid nitrogen and ground into a fine powder with liquid nitrogen using a mixer mills (MM301, Retsh, Haan, Germany) at a frequency of 30 Hz for 30 s. The fresh powders were stored at − 80 °C until analyses. Two additional sets of samples, located next to the analysed samples, were collected. One set was frozen in liquid nitrogen, stored at − 80 °C and used to determine the fresh mass and to estimate the diameter and volume of the stem sections. The other set was used to determine the water content of the stems by differences between the fresh weight measured at the time of sampling and the dry weight measured after 5 days in the oven at 70 °C. The height of each plant was evaluated from photographs taken at the time of sampling.

Chemicals

Methanol (MeOH, LC–MS grade, ≥ 99.9%) was purchased from Honeywell (Charlotte, NC, USA). Chloroform (CHCl3 stabilized with ethanol) and hexane (both for analysis, 99+%), ethanol absolute (EtOH, laboratory regeant grade), acetonitrile (ACN, LC–MS grade, ≥ 99.9%) and formic acid (FA, LC–MS grade) were purchased from Thermo Fisher Scientific (Waltham, MA, USA). Sulfuric acid (H_2SO_4, ACS reagent, 95.0–98.0%) and sodium chloride (NaCl, ≥ 99.5%) were purchased from Sigma Aldrich (St. Louis, MO, USA). Ultra-pure water was obtained from a Milli-Q system (Merck, Darmstadt, Germany) with a resistance of 18.2 MΩ.cm^{-1} at 25 °C. Standard substances used for identification were of analytical grade and purchased from different suppliers.

Metabolite extraction

Extraction of frozen fresh powder (60 mg) was performed for 15 min at 70 °C under constant stirring, with 600 μL of MeOH containing 104.2 μM of ribitol and heptadecanoic acid as internal standards. Then, 450 μL of CHCl3 was added, and the samples were incubated while stirring for 10 min at 37 °C. Finally, 650 μL of H_2O was added. Samples were centrifuged at 21,600 *g* for 5 min at 4 °C. Both solvent phases were collected and analysed. The upper phase containing water and methanol was used for the analysis of primary metabolites, amino acids, polyamines, phenolic compounds and glycoalkaloids. The lower phase containing chloroform was used for the analysis of phytosterols. To exhaust the matrix, the extraction was performed twice on the same powder, and fractions were pooled before analysis. All collected extracts were stored at − 80 °C until analysis. Polar extracts were filtered before analysis using 0.20 μm filters with a 4 mm PTFE hydrophilic membrane (Milles-LG, Merck KGaA, Darmstadt, Germany).

Metabolite analyses

GC−MS and LC−MS analyses were performed as previously described (Dumont et al. 2020). The complete list of metabolites and their identification and quantification parameters are provided in Supplementary Tables S1 and S2.

GC−EI−TOF analyses

Data acquisition was performed on a 7890B GC System (Agilent Technologies, Santa Clara, CA, USA) fit out with MultiPurpose Sampler (Gerstel GmbH & Co, Mülheim, Germany), split/splitless injector, Zebron ZB-SemiVolatiles 34.590 m × 0.25 mm × 0.25 µm column (Phenomenex, Torrance, CA, USA) and Pegasus BT TOF mass spectrometer (LECO, St. Joseph, MI, USA). The MultiPurpose Sampler was controlled by Maestro Version 1.4.40.1 (Gerstel GmbH & Co, Mülheim, Germany) and gas chromatography system with mass spectrometer were controlled by ChromaTOF Version 5.20.38.0.54864 (LECO, Saint Joseph, MI, USA).

Polar extracts were derivatized online before injection: 50 µL of the extract was dried, then incubated in 50 µL of a pyridine solution containing 20 mg·mL^{-1} of methoxyamine hydrochloride under constant shaking at 600 rpm and 80 °C for 30 min. Then, 80 µL of BSTFA containing a mixture of 9 n-alkanes (14 µM decane, 29.3 µM dodecane, 0.3 µM pentadecane, 21.6 µM octadecane, 18.6 µM nonadecane, 19.3 µM docosane, 27.8 µM octacosane, 25.9 µM dotriacontane and 18.7 µM hexatriacontane) were added before heating for 30 min at 80 °C under constant shaking at 600 rpm.

Apolar extract was derivatized online before injection: 50 µL of extract were dried and 50 µL of pyridine followed by 100 µL of BSTFA containing a mixture of 9 n-alkanes (14 µM decane, 29.3 µM dodecane, 0.3 µM pentadecane, 21.6 µM octadecane, 18.6 µM nonadecane, 19.3 µM docosane, 27.8 µM octacosane, 25.9 µM dotriacontane and 18.7 µM hexatriacontane) were added before heating for 30 min at 80 °C under constant shaking at 600 rpm.

One microliter of the sample was injected in splitless mode at 270 °C. Helium was used as carrier gas at 1.0 mL·min^{-1}. The initial oven temperature was kept at 70 °C for 1 min and then increased to 220 °C at a rate of 9 °C.min^{-1}, and then increased to 330 °C at a rate of 15 °C·min^{-1} and maintained for 5 min. The m/z scan range was 50–630 with a cycle time of 10 scans.s^{-1} and an acquisition delay of 310 s. Source temperature and transfer line were set at 250 °C.

UPLC–DAD–ESI–TQ analyses

Data acquisition was performed with an Acquity I-Class UPLC system (Waters, Milford, MA, USA) hyphenated to a mass spectrometer Xevo TQ-XS (Waters, Milford, MA, USA) equipped with an electrospray ionization source. The system was controlled by MassLynx Version 4.1 (Waters, Milford, MA, USA).

Chromatographic separation of amino acids and polyamines was achieved using an Acquity 1.7 µm BEH C18 UPLC column (50 × 2.1 mm, Waters, Milford, MA, USA) and an Acquity BEH C18 1.7 µm UPLC pre-column (Waters, Milford, MA, USA). Samples were derivatized with 6-aminoquinolyl-N-hydroxysuccinimidyl carbamate (AccQ-Tag Ultra Derivatization Kit, Waters, Milford, MA, USA) according to the manufacturer's instructions. One microliter of the derivatized sample was injected into the chromatographic system. Separation was carried out at a constant temperature of 55 °C and flow rate of 0.7 mL·min^{-1} using H$_2$O:FA 99.9:0.1 v/v (A) and ACN:FA 99.9:0.1 v/v (B) as eluents. The chromatographic gradient started with 99.9% solvent A and changed as follows, 0.54 min: 99.9%, 4.5 min: 96.9%, 6.5 min: 90.9%, 8.5 min: 78.8%, 9.9 min: 40.4%, 10.5 min: 40.4%, 10.6 min: 99.9%, 12 min: 99.9%. The source temperature was set at 150 °C and the desolvation temperature 500 °C. The capillary voltage was set at 3.1 kV. Nitrogen was used as the drying and nebulizing gas at 150 L·h^{-1} for the gas flow and 1000 L·h^{-1} for the desolvation gas flow. Compounds were analysed in negative mode using a Multiple Reactions Monitoring (MRM) method described in Supplementary Table S2.

Chromatographic separation of phenolic compounds was achieved on an Acquity 1.7 µm BEH C18 UPLC column (50 × 2.1 mm, Waters, Milford, MA, USA) and an Acquity HSS T3 1.8 µm UPLC pre-column (Waters, Milford, MA, USA). Two microliters of the sample were injected into the chromatographic system. Separation was carried out at a constant temperature of 35 °C and flow rate of 0.4 mL·min^{-1}, using H$_2$O:FA 99.9:0.1 v/v (A) and ACN:FA 99.9:0.1 v/v (B) as eluents. The chromatographic gradient started with 98% solvent A and changed as follows, 0.5 min: 98%, 6.5 min: 55.5%, 7.5 min: 0%, 9 min: 0%, 9.5 min: 98%, 10 min: 98%. The source temperature was set to 150 °C and the desolvation temperature was set to 500 °C. The capillary voltage was set to 3.10 kV. Nitrogen was used as the drying and nebulizing gas at 150 L·h^{-1} for the gas flow and 1000 L·h^{-1} for the desolvation gas flow. Phenolic compounds were analyzed in negative mode using an MRM method described in Supplementary Table S2.

Chromatographic separation of steroidal glycoalkaloids was achieved using an Acquity 1.7 µm BEH C18 UPLC column (50 × 2.1 mm, Waters, Milford, MA, USA) and an Acquity BEH C18 1.7 µm UPLC pre-column (Waters, Milford, MA, USA). One microliter of the sample was injected into the chromatographic system. Separation was carried out at a constant temperature of 40 °C and flow rate of 0.4 mL·min^{-1} using H$_2$O:FA 99.9:0.1 v/v (A) and ACN:FA 99.9:0.1 v/v (B) as eluents. The chromatographic

gradient started with 95% solvent A and changed as follows, 0.25 min: 95%, 1.25 min: 80%, 3.75 min: 75%, 4.25 min: 75%, 5.50 min: 68%, 5.55 min: 0%, 8.00 min: 0%, 8.05 min: 95%, 11.00 min: 95%. The source temperature was set at 150 °C and the desolvation temperature 550 °C. The capillary voltage was set at 3.2 kV. Nitrogen was used as the drying and nebulizing gas at 150 L·h^{-1} for the gas flow and 1000 L·h^{-1} for the desolvation gas flow. Compounds were analysed in positive mode, using an MRM method described in Supplementary Table S2.

HPLC-FLR amino acids

Major amino acids (aspartic acid, glutamic acid, asparagine, glutamine and proline) were analysed after AccQ-Tag chemical derivatization as described above on an Alliance 2695 HPLC system (Waters, Milford, MA, USA) paired to a 2475 fluorescence detector (Waters, Milford, MA, USA). Chromatographic separation was achieved using AccQ-Tag 4 µm Amino Acid Analysis column (3.9 × 150 mm, Waters, Milford, MA, USA). The chromatography system with fluorescence detector was controlled by Chromeleon Version 7.2.10 (ThermoFisher Scientific, Waltham, MA, USA). Separation was carried out at a constant temperature of 37 °C and flow rate of 1 mL·min^{-1}, using sodium acetate buffer (A), ACN (B) and H$_2$O (C) as eluents. The chromatographic gradient started with 100% solvent A and changed as follows, 1 min: 99% A and 1% B, 16 min: 97% A and 3% B, 22 min: 94% A and 6% B, 37 min: 86% A and 14% B, 42 min: 86% A and 14% B, 50 min: 82% A and 18% B, 51 min: 0% A and 60% B, 54 min: 100% A, 63 min: 100% A. The sodium acetate buffer was prepared daily by mixing 1 L of filtered sodium acetate 140 mM, 964 µL of triethylamine and 1 mL of EDTA 2.7 mM then pH was adjusted to 5.8 using H$_3$PO$_4$ 8.5%. Derivatized amino acids were detected by fluorimetry using an excitation wave length of 250 nm and an emission wave length of 395 nm.

Other analysis

Total glutathione was quantified as the GSSG equivalent by enzymatic assay (Massot et al. 2013). The reduced and oxidized forms of ascorbate were quantified by enzymatic assay (Sérino et al. 2019). Starch was measured by enzymatic assay in glucose equivalents (Biais et al. 2014). Total protein was quantified by the Bradford assay (Biais et al. 2014). The cell wall corresponds to the insoluble material obtained after successive washes with MeOH and acetone and starch determination (Renard et al. 1990).

Data processing

GC−MS data files were converted to be processed for automatic peak integration using the TargetLynx XS module (Waters, Milford, MA, USA). Peak annotation was achieved using the Golm mass spectral and retention index library. A specific extracted ion chromatogram was chosen for each molecule for integration; then, peak areas were normalized against the sample dry weight, the internal standard (ribitol or heptadecanoic acid) and the extraction volume. Peak integration was performed using one iteration of mean smoothing and apex tracking. The full dataset is provided in Supplementary Table S1. The relative amount (semi-quantification) of 102 metabolites was established in the samples: 50 of them were identified at level 1 of confidence, 37 at level 2 and 15 at level 3, according to Sumner et al. (2007) (Supplementary Table S2).

The presence of galactinol in the sample extracts was confirmed by injection of a pure standard. Both the retention time and mass spectrum of the peak eluted at 1469 s matched that of galactinol (Supplementary Fig. S1). Two putative galactinol isomers, U_galactinol_1 and U_galactinol_2 were also found in the sample extracts, displaying high spectrum similarity to galactinol (reverse match of 953 and 955, respectively) with the characteristic presence of the ion 523, tentatively identified as the *myo*-inositol-5 TMS moiety. The presence of raffinose in sample extracts was confirmed by the injection of a reference standard, however, the peak could not be integrated due to its partial co-elution with a more abundant compound putatively identified as the maltotriose, whose mass spectrum is very close to that of raffinose.

Statistics

All data treatments and statistics were computed using R software Version 4.2.1. Data plots of all variables are shown in Supplementary Fig. S2. Given the limited number of biological replicates, data were extensively analysed with multivariate statistics and nonparametric tests. Multivariate analysis was performed using the ropls package (Thévenot et al. 2015). Heatmaps were generated using the Complex-Heatmap package (Gu et al. 2016).

Results and discussion

To cover a maximum of C- and N-compounds from both primary and specialized metabolism, a large dataset was compiled, combining metabolomic analyses carried out by several methods, including LC–MS, GC–MS and enzyme assays, as well as growth characteristics. In total, 110
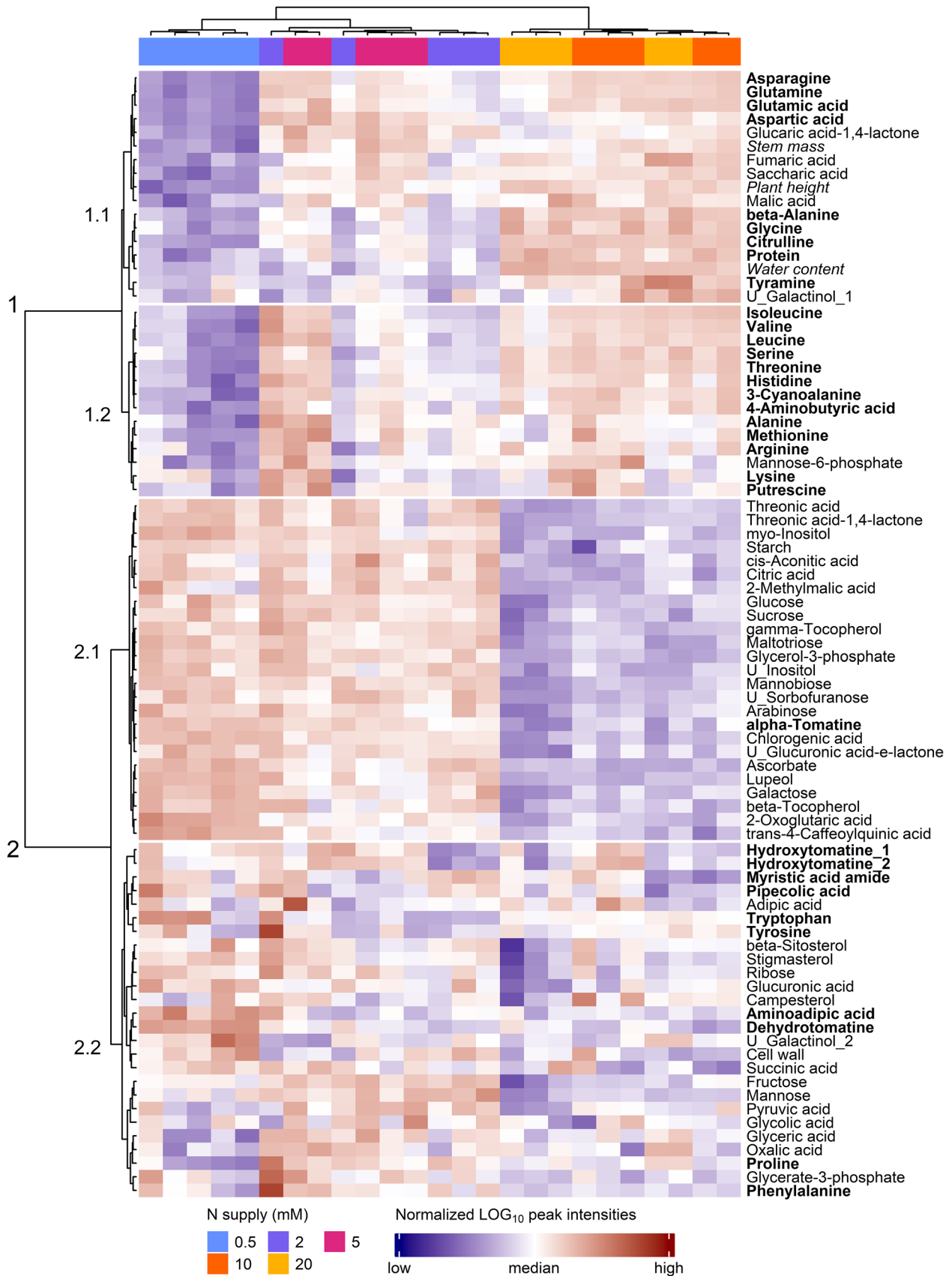
Asparagine
Glutamine
Glutamic acid
Aspartic acid
Glucaric acid-1,4-lactone
Stem mass
Fumaric acid
Saccharic acid
Plant height
Malic acid
beta-Alanine
Glycine
Citrulline
Protein
Water content
Tyramine
U_Galactinol_1

Isoleucine
Valine
Leucine
Serine
Threonine
Histidine
3-Cyanoalanine
4-Aminobutyric acid
Alanine
Methionine
Arginine
Mannose-6-phosphate
Lysine
Putrescine

Threonic acid
Threonic acid-1,4-lactone
myo-Inositol
Starch
cis-Aconitic acid
Citric acid
2-Methylmalic acid
Glucose
Sucrose
gamma-Tocopherol
Maltotriose
Glycerol-3-phosphate
U_Inositol
Mannobiose
U_Sorbofuranose
Arabinose
alpha-Tomatine
Chlorogenic acid
U_Glucuronic acid-e-lactone
Ascorbate
Lupeol
Galactose
beta-Tocopherol
2-Oxoglutaric acid
trans-4-Caffeoylquinic acid

Hydroxytomatine_1
Hydroxytomatine_2
Myristic acid amide
Pipecolic acid
Adipic acid
Tryptophan
Tyrosine
beta-Sitosterol
Stigmasterol
Ribose
Glucuronic acid
Campesterol
Aminoadipic acid
Dehydrotomatine
U_Galactinol_2
Cell wall
Succinic acid
Fructose
Mannose
Pyruvic acid
Glycolic acid
Glyceric acid
Oxalic acid
Proline
Glycerate-3-phosphate
Phenylalanine

N supply (mM)

0.5   2   5
10   20

Normalized LOG$_{10}$ peak intensities

low   median   high

variables including 104 metabolites expressed in relative quantity were analysed to study the effect of *B.cinerea* infection in symptomless tomato stems under several N supplies (Supplementary Table S2).

Low N supply reduced growth and water content and increased the C/N ratio

First, the effect of N nutrition on the metabolic profiles of tomato stems was observed using a hierarchical clustering analysis (HCA) performed on the dataset before inoculation (0 dpi, days post-inoculation) with a subset of the most discriminant variables (top 75% highest VIP, variable importance in the projection returned by a PLS-DA, partial least-squares discriminant analysis), hence discarding noisy variables for the sake of clarity (Fig. 1). The first cluster gathered samples supplied with 0.5, 2 and 5 mM NO_3^- and was associated with lower N-compounds, stem mass, plant height and water content. The impact of N supply on plant physiology is detailed in Supplementary Fig. S3. At up to 10 mM NO_3^-, higher N resulted in higher growth, measured by plant height and stem mass, suggesting a probable limitation in the photosynthetic capacity (Renau-Morata et al. 2021). The stem water content was also significantly higher at 10 and 20 mM NO_3^- than at lower N supply levels, possibly related to the control of root hydraulic conductance through NO_3^- transporters and aquaporins (Cramer et al. 2009; Tyerman et al. 2017). The lowest N supply level, 0.5 mM NO_3^-, formed its own cluster due to distinctive trends in the variables cluster 1.1, including even lower plant height and lower levels of the key amino acids involved in N assimilation and transport, glutamate, glutamine, aspartate and asparagine. In contrast, the second cluster gathered high N supply samples (10 and 20 mM NO_3^-) and was associated with lower C-compounds such as starch, carbohydrates, phytosterols and phenolic compounds (cluster 2.1). All these trends observed 0 dpi were basically conserved 7 dpi (Supplementary Fig. S4).

The decrease in amino acids and proteins and the increase in the levels of starch, most carbohydrates, phosphoesters and secondary metabolites provoked by low N supply were in line with the profiles reported in tomato leaves (Urbanczyk-Wochniak and Fernie 2005). A notable exception was saccharic acid (glucaric acid), which dramatically decreased in plants under very low N supply. The biosynthetic pathway

of this compound, an oxidation product of glucose, has not yet been elucidated in plants, but it is thought to originate from *myo*-inositol and is a precursor of a major phenylpropanoid in tomato, the 2-*O*-caffeoylglucarate (Strack et al. 1987). This particular compound was not detected in our experiment, but C-based secondary metabolites accumulated under N starvation, such as chlorogenic acid, *trans*-4-caffeoylquinic acid, *trans*-5-caffeoylquinic acid and quinic acid, were in agreement with C reallocation towards potential defence compounds (Løvdal et al. 2010; Larbat et al. 2012).

B. cinerea infection symptoms and metabolome changes were negatively correlated with the N supply level

The negative correlation observed between the AUDPC (area under the disease progression curve, as a measure of the severity of symptoms) and N supply confirmed a previous report (Lecompte et al. 2010) (Fig. 2). The largest lesions were found 7 dpi on the plants grown with 0.5 mM NO_3^-, where they expanded rapidly, whereas with 2 and 5 mM NO_3^-, the lesion size was reduced by almost half and exhibited slower expansion rates. The smallest lesions with the lowest expansion rates were found on plants grown with 10 and 20 mM NO_3^-. This distribution revealed three levels of disease susceptibility consistent with the sample clustering based on metabolic profiles observed in Fig. 1. From now on, the 0.5 mM NO_3^- level will thus be referred to as "very-low-N", the levels 2 and 5 mM NO_3^- as "medium-low-N" and 10 and 20 mM NO_3^- as "high-N".

The limited impact of *B. cinerea* inoculation on the metabolome at high-N was confirmed by numbering metabolites significantly affected by the infection. The time points included the following (Mann–Whitney test, *p* value < 0.05): 51 at 0.5 mM NO_3^-, 32 at 2 mM NO_3^-, 41 at 5 mM NO_3^-, and only 11 and 8 at 10 mM NO_3^- and 20 mM NO_3^-, respectively (Supplementary Table S3). More precise pictures of metabolic changes induced by the infection were achieved with orthogonal partial least squares discriminant analysis (OPLS-DA) of the subsets of data representing the three levels of susceptibility (Fig. 3), supplemented by an HCA performed on the OPLS-DA VIPs. At very-low-N and medium-low-N, the OPLS-DA model was good at discriminating mock- and *Botrytis*-inoculated plants ($R^2Y > 0.88$ and $Q^2 > 0.83$), while it failed at high-N ($R^2Y = 0.607$ and $Q^2 = -0.295$), thereby confirming that the metabolome was weakly impacted by the infection in high-N plants. Among the 18 metabolites with significant variation in high-N plants (Supplementary Table S3), only galactinol and alanine showed a clear pattern when examining the full kinetics in Figs. 4a and 5a. In very-low-N and medium-low-N plants, *B. cinerea* triggered the depletion of
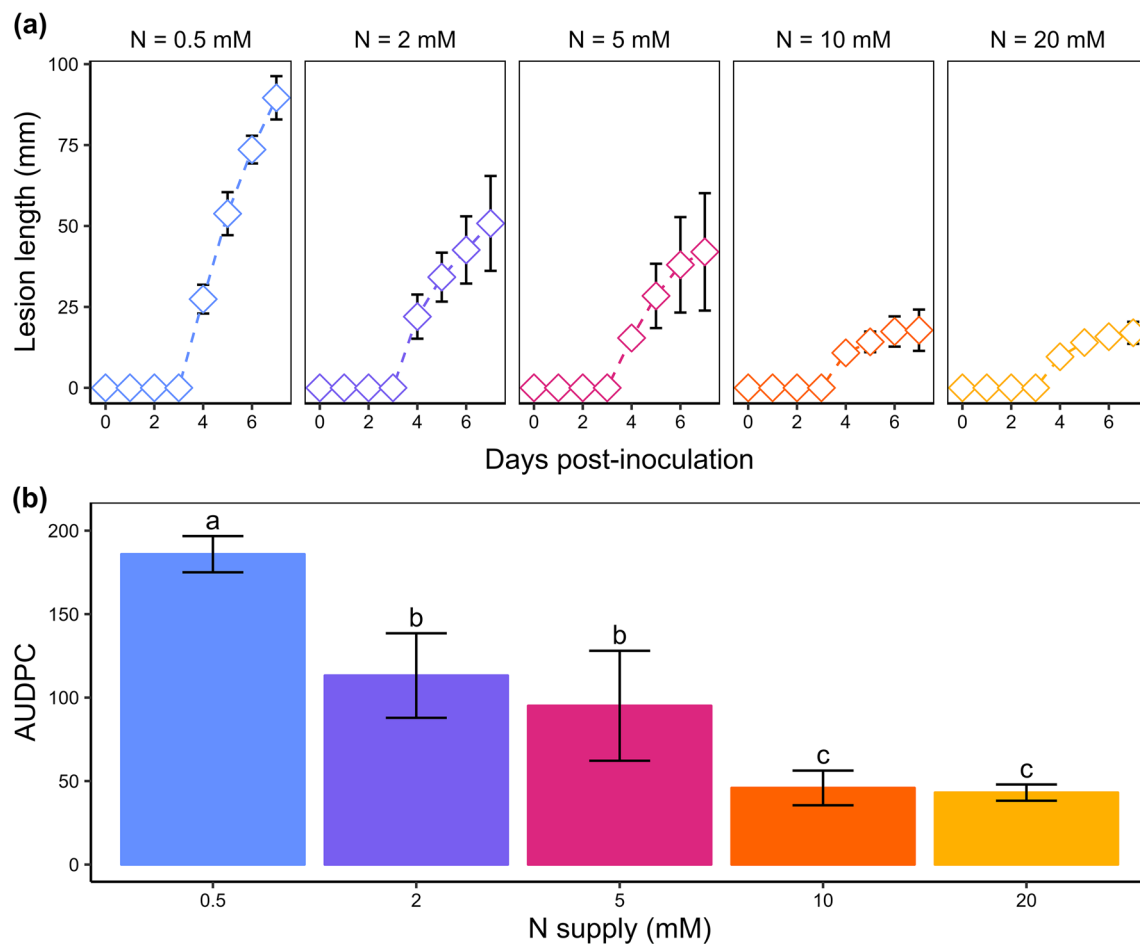
Fig. 2 Disease severity caused by *B. cinerea* on the stem of tomato plants grown upon five levels of N supply. **a** Lesion size on the stems of tomato plants. Each dot represents the mean of five biological replicates, and error bars represent the standard deviation. **b** Area under the disease progress curve (AUDPC) on tomato stems under five different N supplies. Each bar represents the mean of five biological replicates, error bars represent the standard deviation, and letters indicate significant differences between nitrate treatments according to a Kruskal–Wallis test (p value = 0.0003248) followed by a Mann–Whitney–Wilcoxon post hoc test (p value < 0.05)

galactinol, U_galactinol_2 (an unknown galactinol-related molecule), cycloartenol and *myo*-inositol (Fig. 4a, 4c, 4d, 4e) and the accumulation of hexoses-phosphates, glycerate-3-phosphate, 2-oxoglutarate, putrescine, ribose and alanine (Figs. 4h, 4i, 4j, 5a, 5b and Supplementary Fig. S2). An increase in alanine and a decrease in galactinol were thus the only responses common to every plant (Figs. 4a, 5a). Conversely, 4-aminobutyric acid (GABA) accumulation was a specific response in very-low-N plants (Fig. 5d) and branched-chain amino acid (BCAA) accumulation was specific to medium-low-N plants and, more precisely, to plants grown on 5 mM NO_3^- (Fig. 4e–g).

The weak metabolic responses to infection in high-N plants suggest the presence of efficient constitutive defences. Secondary metabolites can be ruled out for this purpose because they were less abundant in resistant plants than in susceptible plants (Figs. 4n, 5h, 5i). On the

other hand, proteins were constitutively far more abundant in resistant plants (Fig. 5j) and could have easily contributed to the rapid setup of defences, such as MAP kinases involved in signalling cascades (Li et al. 2014) or pectin methylesterase inhibitors in Arabidopsis (Lionetti et al. 2017). A lack of proteins in the susceptible plants was thus a serious starting handicap, and N limitation even impaired the subsequent proteome reconfiguration required to establish inducible defences; this was indicated by the limited accumulation of proteins upon infection, which barely reached the constitutive levels found in high-N plants (Fig. 5j). Another probable N-related source of resistance to pathogens is the production of the gaseous radical nitric oxide (NO) by nitrate reductase (NR). NR activity was shown to be regulated by pathogens, as revealed by transcriptomic studies (Vega et al. 2015; Soulie et al. 2020), and NO is part of the defence signalling pathway and a source of resistance against *B. cinerea* (Sivakumaran et al.
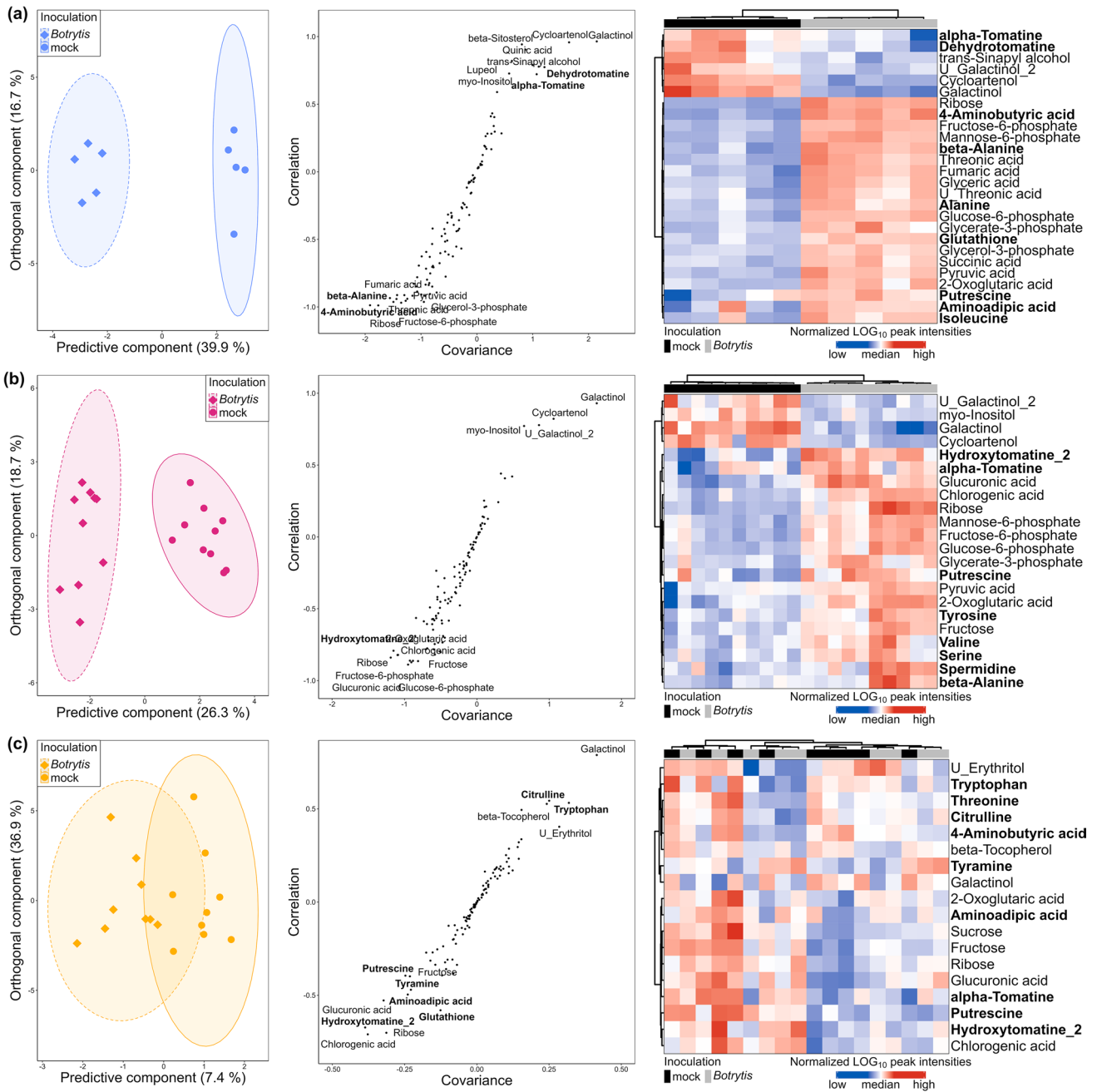
Fig. 3 OPLS-DA of variables measured 7 dpi by *B. cinerea* in the stem of tomato plants grown upon five levels of N supply. Data were log$_{10}$ transformed and Pareto normalized (mean-centred and divided by the root-square of standard deviation). On scores plots (on the left side), ellipses represent the distribution of each group with a 95% level of confidence; the names of the most contributing variables are displayed on S-plots (on the middle). HCA (on the right side) was also performed on the variables with a VIP score > 1.2. **a** Very-low-N samples: on the first predictive component, the goodness-of-fit is $R^2 = 0.94$, and the goodness-of-prediction is $Q^2 = 0.86$. **b** Medium-low-N samples: on the first predictive component, the goodness-of-fit is $R^2 = 0.89$, and the goodness-of-prediction is $Q^2 = 0.83$. **c** High-N samples: on the first predictive component, the goodness-of-fit is $R^2 = 0.61$, and the goodness-of-prediction is $Q^2 = -0.30$. N-compounds are written in bold, and physiological variables are written in italics
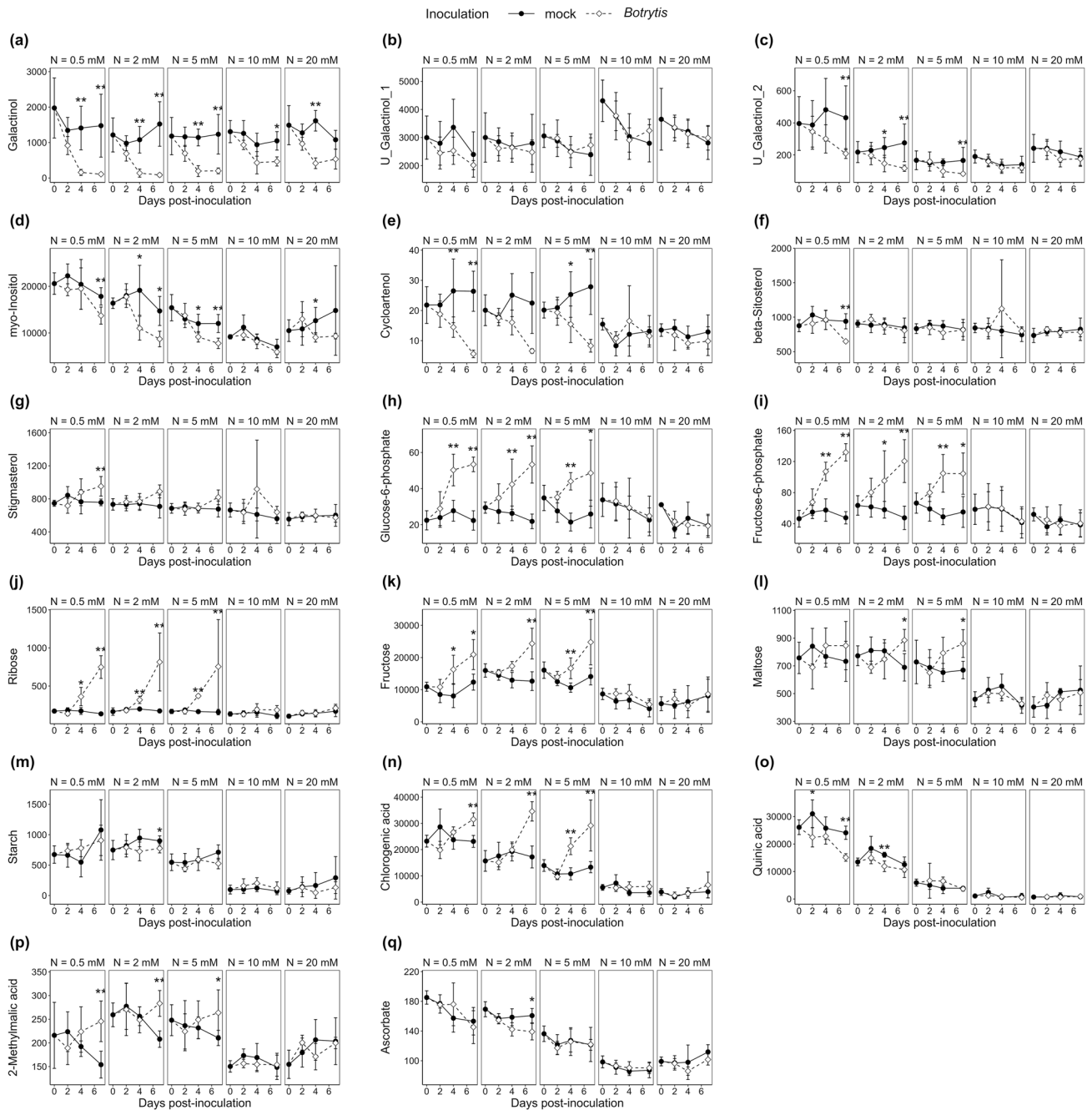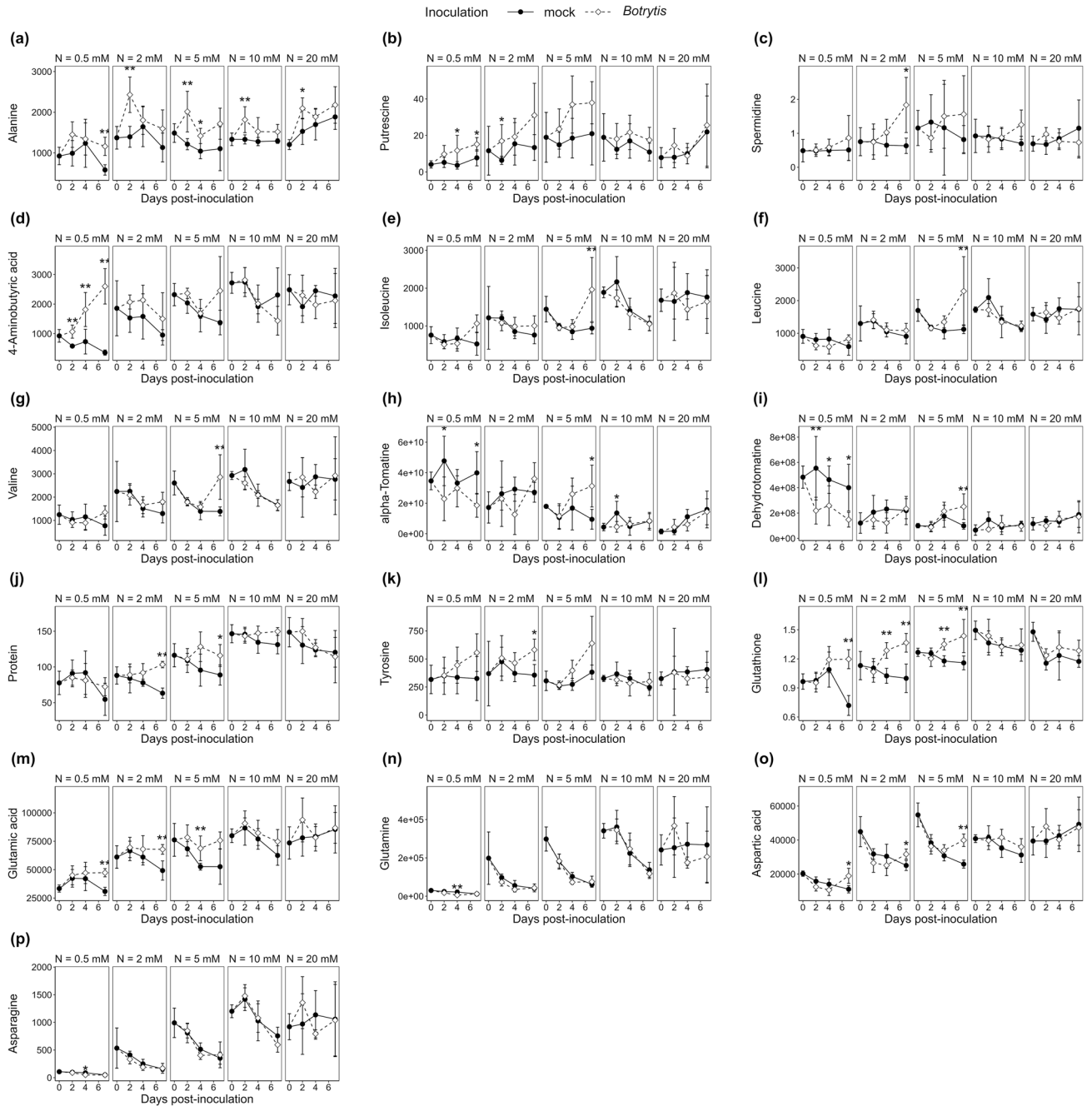
Fig. 4 C-compounds over time in the stem of tomato plants grown upon five levels of N supply and inoculated with mock or *B. cinerea*. Metabolite levels measured over 7 days in symptomless tomato stem sections sampled from plants fertilized with five different nitrate concentrations and inoculated with *B. cinerea* or mock solution. The dif- ferences between mock- and *Botrytis*-inoculated plants were tested at each time point with a Mann–Whitney test. Significant differences are indicated by * ($0.01 < p$ value < 0.05) and ** (p value < 0.01). Black dots and solid lines: mock-inoculated plants; white dots and dotted lines: *Botrytis*-inoculated plants

Fig. 5 N-compounds over time in the stem of tomato plants grown upon five levels of N supply and inoculated with mock or *B. cinerea*. Metabolite levels measured over 7 days in symptomless tomato stem sections sampled from plants fertilized with five different nitrate concentrations and inoculated with *B. cinerea* or mock solution. The differences between mock- and *Botrytis*-inoculated plants were tested at each time point with a Mann–Whitney test. Significant differences are indicated by * ($0.01 < p$ value < 0.05) and ** (p value < 0.01). Black dots and solid lines: mock-inoculated plants; white dots and dotted lines: *Botrytis*-inoculated plants

2016). The low NR activity in plants limited the N supply and therefore probably impaired NO-associated defence mechanisms against *B. cinerea*.

B. cinerea infection triggered galactinol depletion and alanine accumulation regardless of the N supply level

Galactinol was not impacted by N supply, while its direct precursor *myo*-inositol accumulated in very-low-N plants.

After *B. cinerea* inoculation, galactinol levels dropped in all plants, suggesting that molecular aggression, signalling and/or defence processes were well underway in resistant plants, even if they did not result in extensive modulations of the metabolome or show any apparent symptoms. Two unknown galactinol-related molecules, especially U_galactinol_2, dropped only in very-low-N and medium-low-N plants (Fig. 4a–c), as did *myo*-inositol (Fig. 4d).

Galactinol, synthesized from *myo*-inositol and UDP-galactose by a galactinol synthase (GOLS), is an intermediate in the biosynthetic pathway of raffinose family oligosaccharides (RFOs), galactose-containing carbohydrates very common in higher plants. In many plant species, galactinol and RFOs accumulate in response to abiotic stress, including cold, dehydration, and hypersalinity, where they are thought to stabilize membranes and maintain redox homeostasis (Nishizawa et al. 2008; Nishizawa-Yokoi et al. 2008). The literature also supports the involvement of galactinol in defence against pathogens. Tobacco lines overexpressing the cucumber GOLS accumulated up to tenfold more galactinol than the wild type and had up to a 63% higher survival rate when infected by *B. cinerea* (Kim et al. 2008). Moreover, the authors found that a pharmaceutical application of galactinol significantly reduced the diseased lesion areas. Recently, an expression study of three *GOLS* isoforms in *Camellia sinensis* revealed that the transcription of one isoform was upregulated by abiotic stress and abscisic acid (ABA), while the other two were induced by biotic stress, salicylic acid (SA) and jasmonic acid (JA) (Zhou et al. 2017). In addition, *myo*-inositol was proven to be involved in programmed cell death (PCD). Meng et al. (2009) showed that the Arabidopsis mutant *mips1*, with reduced levels of *myo*-inositol and galactinol, developed light and SA-dependent necrotic lesions that could be reversed by *myo*-inositol supplementation. A connection between *myo*-inositol and oxidative stress was found in the *mips1* mutant, which contains lower levels of ascorbic acid and is more susceptible to oxidative stress (Donahue et al. 2010). The mechanism by which *myo*-inositol regulates PCD is not clear, but data suggest the involvement of inositol-phosphoceramide and ceramide homeostasis (Wang et al. 2008). Since cell death is a major component of the hypersensitive response (HR), which is highjacked by necrotrophic fungi to promote their growth (Pitsili et al. 2020), *myo*-inositol and galactinol metabolism might participate in the regulation of redox status and PCD during necrotrophic infection. The drop in galactinol levels, independent of the resistance induced by N supply, supports the hypothesis of an important and mostly unexplored function of this pathway in response to *B. cinerea*.

The only other compound to display significant variations under every N supply level was alanine, with a rapid increase after inoculation followed by a relative decrease (Fig. 5a). Alanine is reversibly synthesized from pyruvate by the transfer of an amino group from glutamate catalyzed by alanine aminotransferases. This amino acid was found to accumulate in Arabidopsis shoots and roots during hypoxic stress and then decrease when returning to optimal O_2 concentrations, due to the activation of *ALAT1* and *ALAT2* (Miyashita et al. 2007). A model of alanine shunt has been proposed, stipulating that hypoxia leads rapidly to insufficient ATP production, triggering the less efficient alcoholic fermentation for NAD^+ regeneration intended to sustain glycolysis and ATP supply (Diab and Limami 2016). An ALAT/GOGAT (glutamine-2-oxoglutarate amino transferase) cycle would mitigate the C depletion of the fermentative pathway that could eventually lead to cell death, by channeling the pyruvate toward alanine accumulation (Limami et al. 2008). Alanine synthesis would store C and N to remove them from the fermentation pathway and restore 2-oxoglutarate replenishing the TCA cycle, while the GOGAT activity would regenerate glutamate and produce NAD^+ for glycolysis. Interestingly, infection by the necrotrophs *B. cinerea* and *Alternaria brassicicola*, but not the hemibiotroph *Pseudomonas syringae*, has been recently shown to trigger local hypoxic stress in Arabidopsis leaves (Valeri et al. 2021) via increased respiration in inoculated leaves: the hypoxia resulted from faster O_2 consumption due to three folds increased respiration in *Botrytis*- than in mock-inoculated leaves. This could be indicative of a strong fungal metabolism promoting both its growth and oxidative activity to produce ROS facilitating its expansion. The relationship between hypoxia and defence against *B. cinerea* has been further supported by the dual role of the transcription factors RAP2.2 and WRKY33 involved in the response to both hypoxia and *B. cinerea* (Zhao et al. 2012; Tang et al. 2021). A possible explanation for alanine accumulation could thus be hypoxia occurring near the site of infection.

Putative defence-related metabolisms were triggered in susceptible plants upon *B. cinerea* infection

Phenolic compounds

While tryptophan, phenylalanine and the most abundant phenolic compound, rutin, remained quite stable upon infection (Supplementary Fig. S2), a few compounds displayed specific variations in very-low-N and medium-low-N plants, such as tyrosine (Fig. 5k), whose accumulation in stems has already been observed after the application of plant growth-promoting rhizobacteria. Moreover, tyrosine-derived tyramine phenolic conjugates, such as feruloyl-tyramine glycosides, have been detected in tomato (Mhlongo 2020). Large amounts of chlorogenic acid accumulated, especially at medium-low-N, while its precursor quinic acid decreased (Fig. 4n, 4o). Chlorogenic acid is a major

secondary metabolite found in every part of tomato plants, including stems (Kim et al. 2014), with direct antifungal activity (Martínez et al. 2017). *Trans*-sinapyl alcohol, the precursor of S lignin, decreased, especially at very-low-N. This could mean an accelerated consumption of sinapyl alcohol to produce lignin since in wheat, a highly localized tenfold increase in sinapyl alcohol dehydrogenase activity was observed in lignifying tissues after elicitation (Mitchell et al. 1994).

Glycoalkaloids

In mock-inoculated plants, despite their nitrogenous nature, the steroidal glycoalkaloids α-tomatine and dehydrotomatine were more abundant in very-low-N plants (Fig. 5h, 5i), behaving like typical C-compounds, probably because of their very high C/N ratio (Hoffland et al. 1999). After infection, both molecules were depleted in very-low-N plants and accumulated specifically in plants grown upon 5 mM NO_3^-. Hydroxytomatine_2, an isomer of hydroxytomatine, followed a similar trend but accumulated to a greater extent in medium-low-N and even in high-N plants, although not in a statistically significant way (Supplementary Fig. S2). Glycoalkaloids have been found in every part of the tomato plant, with the highest content in young leaves, up to 5% of the fresh mass, followed by the stem, where the α-tomatine concentration is three times lower (Kim et al. 2014). However, the involvement of α-tomatine metabolism in resistance to pathogenic fungi is generally thought to be limited because fungi degrade it to less toxic tomatidine by full deglycosylation (Sandrock and VanEtten 1998). Most *B. cinerea* strains also exhibit another type of tomatinase activity by removing the xylose moiety and releasing β1-tomatine (Quidde et al. 1998). Such mechanisms could explain the reduction in α-tomatine and dehydrotomatine observed in very-low-N plants.

Polyamines and GABA

In our experiment, after inoculation, putrescine and spermidine accumulated over time in very-low-N and medium-low-N plants (Fig. 5b, 5c), whereas GABA only accumulated in very-low-N plants, reaching the constitutive level measured in high-N plants 7 dpi (Fig. 5d). This is consistent with reports of polyamine accumulation for several days after *B. cinerea* infection, both in the necrotic spot and in adjacent pathogen-free tissues (Marina et al. 2008; Nambeesan et al. 2012; van Rensburg et al. 2021). The physiological significance of polyamines in plant−pathogen interactions seems to depend on the pathogen lifestyle: beneficial against biotrophs and detrimental against necrotrophs (Marina et al. 2008). Confusing results have been reported thus far when using transgenic lines and exogenous polyamine

applications. Nambeesan et al. (2012) suggested a pro-PCD action of spermidine favourable to the pathogen. On the other hand, an arginine decarboxylase-silenced Arabidopsis line displayed drastically reduced polyamine levels and was also more susceptible to *B. cinerea*. Pretreatment of Arabidopsis plants sprayed with polyamines proved to prime resistance against *B. cinerea*, but higher concentrations provoked cell death (van Rensburg et al. 2021), while tobacco leaf disc infiltrations with polyamines before *Sclerotinia sclerotiorum* inoculation increased the subsequent lesion size (Marina et al. 2008). These contradictions might be due to the amounts of polyamines accumulated and their nature; the tetraamine spermine was more effective than spermidine in priming Arabidopsis resistance (van Rensburg et al. 2021) but was not detected in our samples.

The early accumulation of GABA and succinic acid in very-low-N plants (Fig. 5d and Supplementary Fig. S2) could be interpreted as a rapid activation of the GABA shunt, ensuring the constant replenishment of the TCA cycle to handle defence-associated costs (Li et al. 2021). However, during the interaction of tomato leaf discs and *B. cinerea*, maintenance of cell viability in distal tissues via GS/GOGAT and GABA metabolism was proven crucial for resistance (Seifi et al. 2013). Moreover, exogenous GABA treatment of Arabidopsis leaves showed its priming properties, implicating the control of the ROS burst (van Rensburg and Van den Ende 2020). This antioxidant activity of GABA was found to occur via the regulation of ROS-scavenging enzymes in tomato fruits (Yang et al. 2017).

Branched-chain amino acids (BCAAs)

BCAA levels were constitutively lower under limited N supply but moderately increased 4 dpi in very-low-N plants and more significantly in plants grown in the presence of 5 mM NO_3^- (Fig. 5e, 5f, 5g). The function of BCAA metabolism "as a block" in plant−pathogen interactions is still unknown, but isoleucine is the precursor of two defence-related compounds: (*i*) the bioactive jasmonate-derived jasmonoyl-isoleucine, which is involved in the response to *B. cinerea* (Aubert et al. 2015), and (*ii*) isoleucic acid, which is ubiquitous in the plant kingdom and involved in plant defence (Bauer et al. 2020). In the transcriptomic study published by Vega et al. (2015), the most intensely overexpressed gene in tomato leaves infected by *B. cinerea* encoded threonine dehydratase, the enzyme involved in the first step of isoleucine biosynthesis, confirming that isoleucine plays a particular role in defence. Moreover, we report herein the accumulation of 2-methylmalate (citramalate) in very-low-N and medium-low-N plants after inoculation (Fig. 4p), whose pathway has only been characterized recently in plants (Sugimoto et al. 2021), producing isoleucine from pyruvate and

acetyl-coA, which is a bypass of the aspartate/threonine regular pathway. The contribution of this pathway to defence is unknown.

Glutathione

The levels of glutathione were constitutively higher in high-N plants and strongly increased in very-low-N and medium-low-N plants after inoculation (Fig. 5l). Ascorbate variations, however, were not greatly impacted by *B. cinerea* (Fig. 4q). The only significant difference was a slight reduction observed 7 dpi at 2 mM NO_3^-. These observations are consistent with previous reports by Simon et al. (2013) where, in infected Arabidopsis leaf tissues, *B. cinerea* triggered H_2O_2 accumulation and a drop in the antioxidant system, including ascorbate and glutathione pools, eventually leading to cell death. In the surrounding noninoculated tissues, however, the glutathione content rose gradually but failed to prevent chloroplastic H_2O_2 accumulation 4 dpi. In *Botrytis*-infected tomato leaves, however, no change in total ascorbate and a decrease in total glutathione were observed 5 dpi, whereas in noninoculated leaves, a less pronounced decrease in total glutathione was measured (Kuźniak and Sklodowska 1999). Such variations in ascorbate and glutathione pools were not observed in our work, and overall, the trends suggest a reinforcement of the antioxidant system upon infection, which was constitutive in high-N plants and induced by inoculation in very-low-N and medium-low-N plants.

Phytosterols

After inoculation of very-low-N and medium-low-N plants, we observed a drastic decrease in the level of cycloartenol (Fig. 4e), the first substrate of the phytosterol pathway. Campesterol, stigmasterol and β-sitosterol are the most abundant sterols in plants and important components of the membranes, while cholesterol, also produced from cycloartenol in plants, is usually found in lower amounts except in *Solanaceae*, where it is the precursor of defence steroidal glycoalkaloids (Sonawane et al. 2016). A possible explanation for cycloartenol reduction would be a high consumption rate to feed the biosynthesis of α-tomatine, compensating to some extent for its degradation by the fungus tomatinase and resulting in a net increase of this compound only in medium-low-N plants that have sufficient N resources. At very-low-N, we observed a shift towards stigmasterol accumulation at the expense of β-sitosterol (Fig. 4f, 4g), similar to what was reported in Arabidopsis infected by *Pseudomonas syringae* and *B. cinerea* (Griebel and Zeier 2010), where it correlated with the pathogen-associated molecular pattern (PAMP)- and ROS-triggered

transcriptional induction of *CYP710A1*, a C22 desaturase responsible for most of the sitosterol conversion into stigmasterol. Interestingly, a study of the *cyp710A1* KO mutant showed that stigmasterol accumulation was a susceptibility factor in *Pseudomonas*-infected plants but not in *Botrytis*-infected plants. Subsequent work reported a probable role of *CYP710A1* in the control of nutrient efflux into the apoplast by maintaining membrane integrity (Wang et al. 2012). However, this study reported opposite observations about resistance and suggested that stigmasterol accumulation reflected a plant's attempt to reduce membrane permeability and de facto dry out nutrient transport towards the apoplast.

B. cinerea triggered similar C-compound accumulations in very-low-N and medium-low-N plants but a more limited accumulation of N-compounds

To visualize to what extent plants with severe (0.5 mM NO_3^-) or moderate (5 mM NO_3^-) N limitation were able to quantitatively mobilize metabolic pathways to address the challenge of infection, an HCA was carried out on a selection of variables displaying significant variations 7 dpi after pathogen inoculation, using the ratios of concentrations at either 0.5 or 5 mM NO_3^-, over the concentrations measured at 10 mM NO_3^- (Fig. 6). Cluster 1.2 contained mostly N-compounds with very low constitutive levels in plants severely limited in N (0.5 mM NO_3^-), which only weakly accumulated after inoculation, while they were constitutively more abundant in plants moderately limited in N (5 mM NO_3^-), where they accumulated more strongly after inoculation. These compounds include the total protein fraction, BCAAs, glutamate, aspartate, glutathione and glucuronic acid. Cluster 2.2.1 consists of α-tomatine, dehydrotomatine and hydroxytomatine_1, which accumulated after infection in plants moderately limited in N (5 mM NO_3^-), but decreased in plants severely limited in N (0.5 mM NO_3^-). Cluster 2.1 comprises mostly C-compounds with low constitutive levels in plants severely and moderately limited in N and efficiently accumulated in both after inoculation. This classification suggests that when challenged by the pathogen, plants severely limited in N were able to accumulate C-compounds with the same efficiency as plants moderately limited in N, but not N-compounds. N limitation thus appears to have proportionally restricted N-compounds responding to *B. cinerea*.

An odd result was found concerning the increase in glutamate and aspartate levels upon infection in very-low-N and medium-low-N plants, while glutamine and asparagine remained stable (Fig. 5m–p). Glutamic acid and aspartic acid are well-buffered metabolic hubs; the glutamic acid level in particular is known to remain steady, independent of time of day or nitrogen status, while in contrast, the
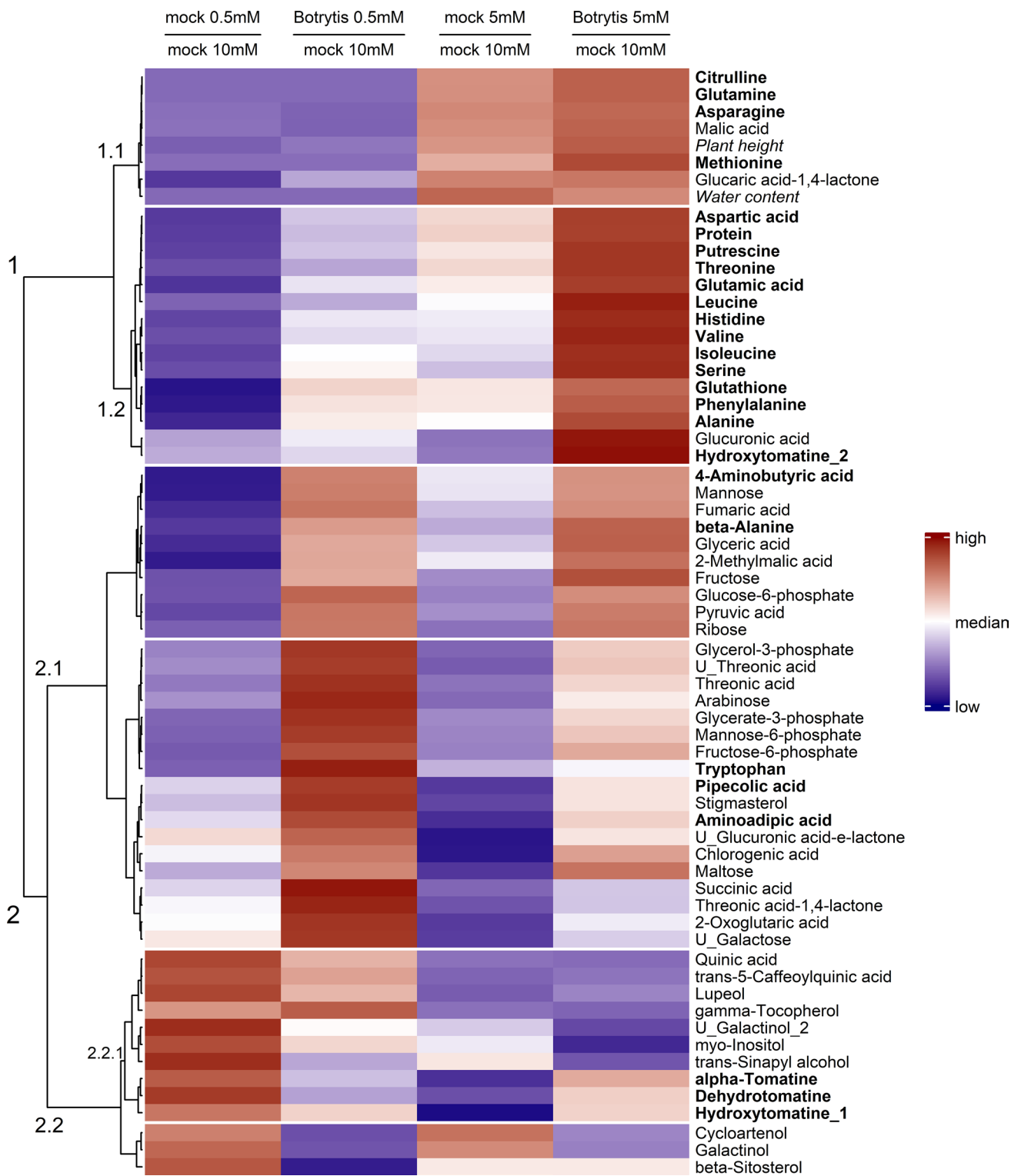
Fig. 6 Hierarchical clustering analysis of a subset of metabolites displaying a significant difference in stem (Mann−Whitney test, *p* value < 0.05) at any time point between *Botrytis*- and mock-inoculated tomato plants upon 0.5 or 5 mM NO_3^-. The columns contain the ratios of concentration at either 0.5 or 5 mM NO_3^- over the concentration measured at 10 mM NO_3^-, 7 dpi. HCA is performed using the Euclidian distance and the Ward algorithm on data after square root transformation and Pareto normalization (mean-centred and divided by the square root of the standard deviation). N-compounds are written in bold, and physiological variables are written in italics

glutamine level displays huge diurnal variations (Scheible et al. 2000) in relation to N assimilation and transportation. Tomato leaves infected by *B. cinerea* have already been found to deplete the asparagine pool through the transcriptional activation of asparagine synthetase (Seifi et al. 2014), an enzyme involved in N remobilization during senescence (Gaufichon et al. 2010). This was interpreted as a sign of pathogen-induced senescence, fuelling the fungus with high quality and quantity of N. Alternatively, Yang et al. (2017) proposed a model placing glutamate metabolism at the core of a survival strategy: plants under necrotrophic attack would enter a state of "endurance" countering cell death and characterized by the preponderance of N translocation towards the site of infection, ROS scavenging and replenishment of the TCA cycle. A consistent observation was made in *Botrytis*-infected sunflower: tissues adjacent to the necrotic spot displayed glutamate depletion (Dulermo et al. 2009), while glutamate dehydrogenase (GDH) transcription was stimulated in the invaded region, suggesting glutamate transfer to invaded regions to delay senescence. In our work, neither the glutamic acid increase nor the protein increase in very-low-N and medium-low-N plants fit with the hypothesis of *Botrytis*-induced senescence or coordinated N transfer towards infected tissues, suggesting that no unequivocal signature of *B. cinerea* infection seems to exist in central N metabolism.

Botrytis cinerea inoculation selectively increased C pools in very-low-N and medium-low-N plants. The starch content was barely affected (Fig. 4m), while a significant accumulation of maltose suggested a possible mobilization of the carbon stocks (Fig. 4l). Fructose accumulated, as well as glycolysis intermediates such as hexose phosphates, glycerate-3-phosphate, and pyruvate, but not sucrose and glucose (Fig. 4h, 4i, 4k and Supplementary Fig. S2). The pentoses arabinose, and especially ribose, also accumulated in very-low-N and medium-low-N plants (Fig. 4j, Supplementary Fig. S2). Interpreting these trends is challenging, given the high flexibility of central metabolism, but they possibly indicate the stimulation of glycolysis, fuelling important sink pathways after infection, such as proteins, chlorogenic acid and α-tomatine, at least in medium-low-N plants. The specific involvement of soluble sugar metabolism in defence has been underlined by many studies [see Meyer et al. (2007) for review], and the singular link between the relative fructose content in tomato stems and susceptibility to *B. cinerea* has been reported by Lecompte et al. (2017). The dramatic fructose increase in plants under low N supply was consistent with the repression of fructokinase genes reported by Lacrampe et al. (2021) and the overexpression of sucrose synthase providing fructose and UDP-glucose, the latter presumed to be consumed in cell wall reinforcement while the former accumulates.

The physiological implications and significance of this fructose accumulation are not clear. High concentrations of fructose in hepatocytes are known to be toxic in relation to the generation of lipids and reactive oxygen species (Kanazawa et al. 2022). However, to our knowledge, no toxic effect of fructose on *B. cinerea* has been reported. A study on the impact of monosaccharides added to the inoculation medium even showed that 3% (w/v) fructose stimulated the infection of *Vicia faba* in a similar way than glucose (Edlich et al. 1989). In plants, a signalling pathway specifically involving fructose and interacting with ABA and ethylene signalling has been demonstrated by Cho and Yoo (2011), implicating the transcription factor ANAC089 (Li et al. 2011), which notably controls endoplasmic reticulum stress-mediated cell death (Yang et al. 2014). A potential link between fructose and the response to biotic stresses was recently suggested by (*i*) the correlations observed between nutrition-induced saccharide levels, including fructose, and hormonal responses as well as disease symptoms during the interaction between the hemibiotroph *Fusarium oxysporum* and Yellow Lupine (Formela-Luboińska et al. 2020)on one hand, and (*ii*) the immune response to an oomycete attack requiring the activation of NAC089 on the other hand (Ai et al. 2021). It is therefore possible that high fructose concentrations participate in a direct or signalling defence mechanism against *B. cinerea*. The transcriptional activity of genes involved in sugar metabolism explored by Lacrampe et al. (2021) showed that at high N, resistance was correlated with the rapid and transient transcriptional activation of mitochondrial hexokinases *HXK1*, *HXK2*, the fructokinases *FRK1*, *FRK2*, *FRK3* and the phosphofructokinase *PFK1*, while the fructokinases where repressed in low-N plants. These results suggested that a high and early C flux into the downstream
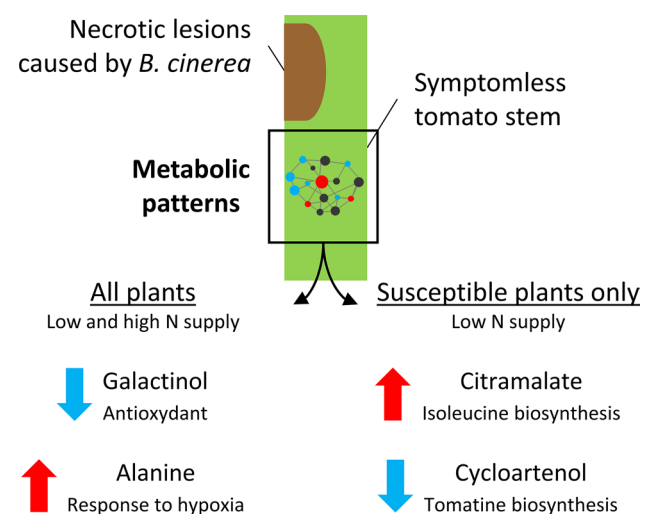

Fig. 7 Involvement of galactinol, alanine, citramalate and cycloartenol in the tomato stem response to *B. cinerea*

glycolysis and pentose phosphate pathways is required for resistance, which failed to happen under N deficiency.

Conclusions

This work is, to our knowledge, the first metabolomic exploration of tomato stems inoculated with *B. cinerea* and reports rather unexpected changes in galactinol, alanine, cycloartenol and citramalate metabolisms (Fig. 7). The limited variations of metabolic pools in high-N resistant plants upon infection underlined the importance of resistance mechanisms developing only under nonlimiting N supply, such as high protein content conferring constitutive defences or superior proteome reconfiguration capabilities after the attack. In contrast, the metabolome of very-low-N and medium-low-N susceptible plants showed symptoms of massive metabolic changes following infection, including no obvious sign of senescence but the activation of several confirmed or more elusive defence systems against necrotrophs, such as accumulation of antimicrobial compounds and antioxidants and reconfigurations of central metabolism with a possible role in systemic oxidative stress control. Overall, the results suggested that symptomless tissues adjacent to the necrotic spot have perceived *B. cinerea* attack and aimed to keep plant cells alive even at low N supply. These responses, however, were unable to provide effective resistance, perhaps because of their limited amplitude or their slow implementation in the context of N deprivation. None of the findings reported here explains the opposite effects of nitrogen deficiency on resistance to *B. cinerea* in different species, such as tomato and Arabidopsis. A direct comparative study would probably be necessary to address this question. Another limitation of this work is the lack of information about the reallocation of metabolic pools from or to other organs since it is a fundamental process occurring in the stems. Future differentiated analysis at finer spatial scales, including analysis of the epidermis, parenchyma, and conducting vessels, would provide a better understanding of these fluxes.

Author contribution statement NL performed all the experiments and metabolomic analyses and contributed to data mining; FL and SC designed the research; DD analysed ascorbate, glutathione, asparagine, glutamine, glutamate, aspartate and proline; RL performed data mining and wrote the article.

Declarations

References

Ai G, Zhu H, Fu X et al (2021) *Phytophthora infection* signals-induced translocation of NAC089 is required for endoplasmic reticulum stress response-mediated plant immunity. Plant J 108:67–80. https://doi.org/10.1111/tpj.15425

Allwood JW, Williams A, Uthe H et al (2021) Unravelling plant responses to stress—the importance of targeted and untargeted metabolomics. Metabolites. https://doi.org/10.3390/metabo11080558

Asselbergh B, Curvers K, França SC et al (2007) Resistance to *Botrytis cinerea* in sitiens, an abscisic acid-deficient tomato mutant, involves timely production of hydrogen peroxide and cell wall modifications in the epidermis. Plant Physiol 144:1863–1877. https://doi.org/10.1104/pp.107.099226

Aubert Y, Widemann E, Miesch L et al (2015) CYP94-mediated jasmonoyl-isoleucine hormone oxidation shapes jasmonate profiles and attenuates defence responses to *Botrytis cinerea* infection. J Exp Bot 66:3879–3892. https://doi.org/10.1093/jxb/erv190

Bauer S, Mekonnen DW, Geist B et al (2020) The isoleucic acid triad: distinct impacts on plant defense, root growth, and formation of reactive oxygen species. J Exp Bot 71:4258–4270. https://doi.org/10.1093/jxb/eraa160

Biais B, Bénard C, Beauvoit B et al (2014) Remarkable reproducibility of enzyme activity profiles in tomato fruits grown under contrasting environments provides a roadmap for studies of fruit metabolism. Plant Physiol 164:1204–1221. https://doi.org/10.1104/pp.113.231241

Bolton MD (2009) Primary metabolism and plant defense—fuel for the fire. Mol Plant-Microbe Interact 22:487–497. https://doi.org/10.1094/MPMI-22-5-0487

Camañes G, Scalschi L, Vicedo B et al (2015) An untargeted global metabolomic analysis reveals the biochemical changes underlying basal resistance and priming in *Solanum lycopersicum*, and

identifies 1-methyltryptophan as a metabolite involved in plant responses to *Botrytis cinerea* and *Pseudomonas syringae*. Plant J 84:125–139. https://doi.org/10.1111/tpj.12964

Chen S, Fu Y, Peng X et al (2021) *Trichoderma harzianum* enhances resistance to *Botrytis cinerea* by promoting photosynthesis, redox homeostasis and secondary metabolites in tomato. SSRN. https://doi.org/10.2139/ssrn.3990631

Cho Y-H, Yoo S-D (2011) Signaling role of fructose mediated by FINS1/FBP in *Arabidopsis thaliana*. PLoS Genet 7:e1001263. https://doi.org/10.1371/journal.pgen.1001263

Choquer M, Fournier E, Kunz C et al (2007) *Botrytis cinerea* virulence factors: new insights into a necrotrophic and polyphageous pathogen. FEMS Microbiol Lett 277:1–10. https://doi.org/10.1111/j.1574-6968.2007.00930.x

Cramer MD, Hawkins HJ, Verboom GA (2009) The importance of nutritional regulation of plant water flux. Oecologia 161:15–24. https://doi.org/10.1007/s00442-009-1364-3

De Cremer K, Mathys J, Vos C et al (2013) RNAseq-based transcriptome analysis of *Lactuca sativa* infected by the fungal necrotroph *Botrytis cinerea*. Plant Cell Environ 36:1992–2007. https://doi.org/10.1111/pce.12106

Diab H, Limami AM (2016) Reconfiguration of N metabolism upon hypoxia stress and recovery: roles of alanine aminotransferase (AlaAt) and glutamate dehydrogenase (GDH). Plants 5:345–367. https://doi.org/10.3390/plants5020025

Donahue JL, Alford SR, Torabinejad J et al (2010) The *Arabidopsis thaliana* myo-inositol 1-phosphate synthase1 gene is required for myo-inositol synthesis and suppression of cell death. Plant Cell 22:888–903. https://doi.org/10.1105/tpc.109.071779

Dulermo T, Bligny R, Gout E, Cotton P (2009) Amino acid changes during sunflower infection by the necrotrophic fungus *B. cinerea*. Plant Signal Behav 4:859–861. https://doi.org/10.4161/psb.4.9.9397

Dumont D, Danielato G, Chastellier A et al (2020) Multi-targeted metabolic profiling of carotenoids, phenolic compounds and primary metabolites in goji (*Lycium* spp.) berry and tomato (*Solanum lycopersicum*) reveals inter and intra genus biomarkers. Metabolites 10:1–17. https://doi.org/10.3390/metabo10100422

Edlich W, Lorenz G, Lyr H et al (1989) New aspects on the infection mechanism of *Botrytis cinerea Pers*. Netherlands J Plant Pathol 95:53–62. https://doi.org/10.1007/BF01974284

Fagard M, Launay A, Clément G et al (2014) Nitrogen metabolism meets phytopathology. J Exp Bot 65:5643–5656. https://doi.org/10.1093/jxb/eru323

Feussner I, Polle A (2015) What the transcriptome does not tell—proteomics and metabolomics are closer to the plants' pathophenotype. Curr Opin Plant Biol 26:26–31. https://doi.org/10.1016/j.pbi.2015.05.023

Formela-Luboińska M, Chadzinikolau T, Drzewiecka K et al (2020) The role of sugars in the regulation of the level of endogenous signaling molecules during defense response of yellow lupine to *Fusarium oxysporum*. Int J Mol Sci 21:4133. https://doi.org/10.3390/ijms21114133

Friedman M (2002) Tomato glycoalkaloids: role in the plant and in the diet. J Agric Food Chem 50:5751–5780. https://doi.org/10.1021/jf020560c

Gao P, Zhang H, Yan H et al (2021) RcTGA1 and glucosinolate biosynthesis pathway involvement in the defence of rose against the necrotrophic fungus *Botrytis cinerea*. BMC Plant Biol 21:1–17. https://doi.org/10.1186/s12870-021-02973-z

Gaufichon L, Reisdorf-Cren M, Rothstein SJ et al (2010) Biological functions of asparagine synthetase in plants. Plant Sci 179:141–153. https://doi.org/10.1016/j.plantsci.2010.04.010

Griebel T, Zeier J (2010) A role for β-sitosterol to stigmasterol conversion in plant-pathogen interactions. Plant J 63:254–268. https://doi.org/10.1111/j.1365-313X.2010.04235.x

Gu Z, Eils R, Schlesner M (2016) Complex heatmaps reveal patterns and correlations in multidimensional genomic data. Bioinformatics 32:2847–2849. https://doi.org/10.1093/bioinformatics/btw313

Heil M, Baldwin IT (2002) Fitness costs of induced resistance: emerging experimental support for a slippery concept. Trends Plant Sci 7:61–67. https://doi.org/10.1016/S1360-1385(01)02186-0

Hoffland E, Van Beusichem ML, Jeger MJ (1999) Nitrogen availability and susceptibility of tomato leaves to *Botrytis cinerea*. Plant Soil 210:263–272. https://doi.org/10.1023/A:1004661913224

Holz G, Coertze S, Williamson B (2007) The ecology of *Botrytis* on plant surfaces. Botrytis Biol Pathol Control. https://doi.org/10.1007/978-1-4020-2626-3_2

Hong Y-S, Martinez A, Liger-Belair G et al (2012) Metabolomics reveals simultaneous influences of plant defence system and fungal growth in *Botrytis cinerea*-infected *Vitis vinifera* cv. Chardonnay berries. J Exp Bot 63:5773–5785. https://doi.org/10.1093/jxb/ers228

Kanazawa J, Kakisaka K, Suzuki Y et al (2022) Excess fructose enhances oleatic cytotoxicity via reactive oxygen species production and causes necroptosis in hepatocytes. J Nutr Biochem 107:109052. https://doi.org/10.1016/j.jnutbio.2022.109052

Kim MS, Cho SM, Kang EY et al (2008) Galactinol is a signaling component of the induced systemic resistance caused by *Pseudomonas chlororaphis* O6 root colonization. Mol Plant-Microbe Interact 21:1643–1653. https://doi.org/10.1094/MPMI-21-12-1643

Kim DS, Na H, Kwack Y, Chun C (2014) Secondary metabolite profiling in various parts of tomato plants. Korean J Hortic Sci Technol 32:252–260. https://doi.org/10.7235/hort.2014.13165

Kuźniak E, Sklodowska M (1999) The effect of *Botrytis cinerea* infection on ascorbate-glutathione cycle in tomato leaves. Plant Sci 148:69–76. https://doi.org/10.1016/S0168-9452(99)00121-1

Lacrampe N, Lopez-Lauri F, Lugan R et al (2021) Regulation of sugar metabolism genes in the nitrogen-dependent susceptibility of tomato stems to *Botrytis cinerea*. Ann Bot 127:143–154. https://doi.org/10.1093/aob/mcaa155

Larbat R, Le Bot J, Bourgaud F et al (2012) Organ-specific responses of tomato growth and phenolic metabolism to nitrate limitation. Plant Biol 14:760–769. https://doi.org/10.1111/j.1438-8677.2012.00564.x

Lecompte F, Abro MA, Nicot PC (2010) Contrasted responses of *Botrytis cinerea* isolates developing on tomato plants grown under different nitrogen nutrition regimes. Plant Pathol 59:891–899. https://doi.org/10.1111/j.1365-3059.2010.02320.x

Lecompte F, Abro MA, Nicot PC (2013) Can plant sugars mediate the effect of nitrogen fertilization on lettuce susceptibility to two necrotrophic pathogens: *Botrytis cinerea* and *Sclerotinia sclerotiorum*? Plant Soil 369:387–401. https://doi.org/10.1007/s11104-012-1577-9

Lecompte F, Nicot PC, Ripoll J et al (2017) Reduced susceptibility of tomato stem to the necrotrophic fungus *Botrytis cinerea* is associated with a specific adjustment of fructose content in the host sugar pool. Ann Bot 119:931–943. https://doi.org/10.1093/aob/mcw240

Li P, Wind JJ, Shi X et al (2011) Fructose sensitivity is suppressed in *Arabidopsis* by the transcription factor ANAC089 lacking the membrane-bound domain. PNAS 108:3436–3441. https://doi.org/10.1073/pnas.1018665108

Li X, Zhang Y, Huang L et al (2014) Tomato *SlMKK2* and *SlMKK4* contribute to disease resistance against *Botrytis cinerea*. BMC Plant Biol 14:1–17. https://doi.org/10.1186/1471-2229-14-166

Li L, Dou N, Zhang H, Wu C (2021) The versatile GABA in plants. Plant Signal Behav. https://doi.org/10.1080/15592324.2020.1862565

Limami AM, Glévarec G, Ricoult C et al (2008) Concerted modulation of alanine and glutamate metabolism in young *Medicago*

truncatula seedlings under hypoxic stress. J Exp Bot 59:2325–2335. https://doi.org/10.1093/jxb/ern102

Lionetti V, Fabri E, De Caroli M et al (2017) Three pectin methylesterase inhibitors protect cell wall integrity for arabidopsis immunity to *Botrytis*. Plant Physiol 173:1844–1863. https://doi.org/10.1104/pp.16.01185

Løvdal T, Olsen KM, Slimestad R et al (2010) Synergetic effects of nitrogen depletion, temperature, and light on the content of phenolic compounds and gene expression in leaves of tomato. Phytochemistry 71:605–613. https://doi.org/10.1016/j.phytochem.2009.12.014

Marina M, Maiale SJ, Rossi FR et al (2008) Apoplastic polyamine oxidation plays different roles in local responses of tobacco to infection by the necrotrophic fungus *Sclerotinia sclerotiorum* and the biotrophic bacterium *Pseudomonas viridiflava*. Plant Physiol 147:2164–2178. https://doi.org/10.1104/pp.108.122614

Martínez G, Regente M, Jacobi S et al (2017) Chlorogenic acid is a fungicide active against phytopathogenic fungi. Pestic Biochem Physiol 140:30–35. https://doi.org/10.1016/j.pestbp.2017.05.012

Massot C, Bancel D, Lauri FL et al (2013) High temperature inhibits ascorbate recycling and light stimulation of the ascorbate pool in tomato despite increased expression of biosynthesis genes. PLoS ONE 8:1–13. https://doi.org/10.1371/journal.pone.0084474

Meng PH, Raynaud C, Tcherkez G et al (2009) Crosstalks between myo-inositol metabolism, programmed cell death and basal immunity in *Arabidopsis*. PLoS ONE. https://doi.org/10.1371/journal.pone.0007364

Meyer RC, Steinfath M, Lisec J et al (2007) The metabolic signature related to high plant growth rate in *Arabidopsis thaliana*. PNAS USA 104:4759–4764. https://doi.org/10.1073/pnas.0609709104

Mhlongo MI, Piater LA, Steenkamp PA et al (2020) Metabolic profiling of PGPR-treated tomato plants reveal priming-related adaptations of secondary metabolites and aromatic amino acids. Metabolites 10:210. https://doi.org/10.3390/metabo10050210

Mitchell HJ, Hall JL, Barber MS (1994) Elicitor-induced cinnamyl alcohol dehydrogenase activity in lignifying wheat (*Triticum aestivum* L.) leaves. Plant Physiol 104:551–556. https://doi.org/10.1104/pp.104.2.551

Miyashita Y, Dolferus R, Ismond KP, Good AG (2007) Alanine aminotransferase catalyses the breakdown of alanine after hypoxia in *Arabidopsis thaliana*. Plant J 49:1108–1121. https://doi.org/10.1111/j.1365-313X.2006.03023.x

Nambeesan S, AbuQamar S, Laluk K et al (2012) Polyamines attenuate ethylene-mediated defense responses to abrogate resistance to *Botrytis cinerea* in tomato. Plant Physiol 158:1034–1045. https://doi.org/10.1104/pp.111.188698

Nicot P, Bardin M, Debruyne F et al (2013) Effect of nitrogen fertilisation of strawberry plants on the efficacy of defence-stimulating biocontrol products against *Botrytis cinerea*. IOBC-WPRS Bull 88:39–42

Nishizawa A, Yabuta Y, Shigeoka S (2008) Galactinol and raffinose constitute a novel function to protect plants from oxidative damage. Plant Physiol 147:1251–1263. https://doi.org/10.1104/pp.108.122465

Nishizawa-Yokoi A, Yabuta Y, Shigeoka S (2008) The contribution of carbohydrates including raffinose family oligosaccharides and sugar alcohols to protection of plant cells from oxidative damage. Plant Signal Behav 3:1016–1018. https://doi.org/10.4161/psb.6738

Pitsili E, Phukan UJ, Coll NS (2020) Cell death in plant immunity. Cold Spring Harb Perspect Biol. https://doi.org/10.1101/cshperspect.a036483

Quidde T, Osbourn AE, Tudzynski P (1998) Detoxification of α-tomatine by *Botrytis cinerea*. Physiol Mol Plant Pathol 52:151–165. https://doi.org/10.1006/pmpp.1998.0142

Renard CMGC, Voragen AGJ, Thibault JF, Pilnik W (1990) Studies on apple protopectin: I. Extraction of insoluble pectin by chemical means. Carbohydr Polym 12:9–25. https://doi.org/10.1016/0144-8617(90)90101-W

Renau-Morata B, Molina RV, Minguet EG et al (2021) Integrative transcriptomic and metabolomic analysis at organ scale reveals gene modules involved in the responses to suboptimal nitrogen supply in tomato. Agronomy. https://doi.org/10.3390/agronomy11071320

Rossi FR, Krapp AR, Bisaro F et al (2017) Reactive oxygen species generated in chloroplasts contribute to tobacco leaf infection by the necrotrophic fungus *Botrytis cinerea*. Plant J 92:761–773. https://doi.org/10.1111/tpj.13718

Sandrock RW, VanEtten HD (1998) Fungal sensitivity to and enzymatic degradation of the phytoanticipin α-tomatine. Phytopathology 88:137–143. https://doi.org/10.1094/PHYTO.1998.88.2.137

Scheible WR, Krapp A, Stitt M (2000) Reciprocal diurnal changes of phosphoenolpyruvate carboxylase expression and cytosolic pyruvate kinase, citrate synthase and NADP-isocitrate dehydrogenase expression regulate organic acid metabolism during nitrate assimilation in tobacco leaves. Plant Cell Environ 23:1155–1167. https://doi.org/10.1046/j.1365-3040.2000.00634.x

Seifi HS, Curvers K, De Vleesschauwer D et al (2013) Concurrent overactivation of the cytosolic glutamine synthetase and the GABA shunt in the ABA-deficient sitiens mutant of tomato leads to resistance against *Botrytis cinerea*. New Phytologist 199:490–504. https://doi.org/10.1111/nph.12283

Seifi HS, De Vleesschauwer D, Aziz A, Höfte M (2014) Modulating plant primary amino acid metabolism as a necrotrophic virulence strategy. Plant Signal Behav 9:e27995. https://doi.org/10.4161/psb.27995

Sérino S, Costagliola G, Gomez L (2019) Lyophilized tomato plant material: validation of a reliable extraction method for the analysis of vitamin C. J Food Compos Anal 81:37–45. https://doi.org/10.1016/j.jfca.2019.05.001

Simon UK, Polanschütz LM, Koffler BE, Zechmann B (2013) High resolution imaging of temporal and spatial changes of subcellular ascorbate, glutathione and H_2O_2 distribution during *Botrytis cinerea* infection in *Arabidopsis*. PLoS ONE 8:e65811. https://doi.org/10.1371/journal.pone.0065811

Sivakumaran A, Akinyemi A, Mandon J et al (2016) ABA suppresses *Botrytis cinerea* elicited NO production in tomato to influence H_2O_2 generation and increase host susceptibility. Front Plant Sci 7:1–12. https://doi.org/10.3389/fpls.2016.00709

Sonawane PD, Pollier J, Panda S et al (2016) Plant cholesterol biosynthetic pathway overlaps with phytosterol metabolism. Nat Plants. https://doi.org/10.1038/nplants.2016.205

Soulie MC, Koka SM, Floch K et al (2020) Plant nitrogen supply affects the *Botrytis cinerea* infection process and modulates known and novel virulence factors. Mol Plant Pathol 21:1436–1450. https://doi.org/10.1111/mpp.12984

Stare T, Stare K, Weckwerth W et al (2017) Comparison between proteome and transcriptome response in potato (*Solanum tuberosum* L.) leaves following potato virus Y (PVY) infection. Proteomes 5:14. https://doi.org/10.3390/proteomes5030014

Strack D, Gross W, Wray V, Grotjahn L (1987) Enzymic synthesis of caffeoylglucaric acid from chlorogenic acid and glucaric acid by a protein preparation from tomato cotyledons. Plant Physiol 83:475–478. https://doi.org/10.1104/pp.83.3.475

Sugimoto N, Engelgau P, Daniel Jones A et al (2021) Citramalate synthase yields a biosynthetic pathway for isoleucine and straight- and branched-chain ester formation in ripening apple fruit. PNAS USA. https://doi.org/10.1073/pnas.2009988118

Sumner LW, Amberg A, Barrett D et al (2007) Proposed minimum reporting standards for chemical analysis. Metabolomics 3:211–221. https://doi.org/10.1007/s11306-007-0082-2

Tang H, Bi H, Liu B et al (2021) WRKY33 interacts with WRKY12 protein to up-regulate RAP2.2 during submergence induced hypoxia response in *Arabidopsis thaliana*. New Phytol 229:106–125. https://doi.org/10.1111/nph.17020

Thévenot EA, Roux A, Xu Y et al (2015) Analysis of the human adult urinary metabolome variations with age, body mass index, and gender by implementing a comprehensive workflow for univariate and OPLS statistical analyses. J Proteome Res 14:3322–3335. https://doi.org/10.1021/acs.jproteome.5b00354

Tyerman SD, Wignes JA, Kaiser BN (2017) Root hydraulic and aquaporin responses to N availability. Signal Commun Plants. https://doi.org/10.1007/978-3-319-49395-4_10

Urbanczyk-Wochniak E, Fernie AR (2005) Metabolic profiling reveals altered nitrogen nutrient regimes have diverse effects on the metabolism of hydroponically-grown tomato (*Solanum lycopersicum*) plants. J Exp Bot 56:309–321. https://doi.org/10.1093/jxb/eri059

Valeri MC, Novi G, Weits DA et al (2021) *Botrytis cinerea* induces local hypoxia in *Arabidopsis* leaves. New Phytol 229:173–185. https://doi.org/10.1111/nph.16513

Van Baarlen P, Woltering EJ, Staats M, Van Kan JAL (2007) Histochemical and genetic analysis of host and non-host interactions of *Arabidopsis* with three *Botrytis* species: an important role for cell death control. Mol Plant Pathol 8:41–54. https://doi.org/10.1111/j.1364-3703.2006.00367.x

van Rensburg HCJ, Van den Ende W (2020) Priming with γ-aminobutyric acid against *Botrytis cinerea* reshuffles metabolism and reactive oxygen species: dissecting signalling and metabolism. Antioxidants 9:1–22. https://doi.org/10.3390/antiox9121174

van Rensburg HCJ, Limami AM, Van den Ende W (2021) Spermine and spermidine priming against *Botrytis cinerea* modulates ros dynamics and metabolism in *Arabidopsis*. Biomolecules 11:1–25. https://doi.org/10.3390/biom11020223

Vega A, Canessa P, Hoppe G et al (2015) Transcriptome analysis reveals regulatory networks underlying differential susceptibility to *Botrytis cinerea* in response to nitrogen availability in *Solanum lycopersicum*. Front Plant Sci 6:1–17. https://doi.org/10.3389/fpls.2015.00911

Wang W, Yang X, Tangchaiburana S et al (2008) An inositolphosphorylceramide synthase is involved in regulation of plant programmed cell death associated with defense in *Arabidopsis*. Plant Cell 20:3163–3179. https://doi.org/10.1105/tpc.108.060053

Wang K, Senthil-Kumar M, Ryu CM et al(2012) Phytosterols play a key role in plant innate immunity against bacterial pathogens by regulating nutrient efflux into the apoplast. Plant Physiol 158:1789–1802. https://doi.org/10.1104/pp.111.189217

Windram O, Madhou P, Mchattie S et al (2012) *Arabidopsis* defense against *Botrytis cinerea*: chronology and regulation deciphered by high-resolution temporal transcriptomic analysis. Plant Cell 24:3530–3557. https://doi.org/10.1105/tpc.112.102046

Yang Z-T, Wang M-J, Sun L et al (2014) The membrane-associated transcription factor NAC089 controls ER-stress-induced programmed cell death in plants. PLoS Genet 10:e1004243. https://doi.org/10.1371/journal.pgen.1004243

Yang J, Sun C, Zhang Y et al (2017) Induced resistance in tomato fruit by γ-aminobutyric acid for the control of alternaria rot caused by *Alternaria alternata*. Food Chem 221:1014–1020. https://doi.org/10.1016/j.foodchem.2016.11.061

Zhao Y, Wei T, Yin KQ et al (2012) *Arabidopsis* RAP2.2 plays an important role in plant resistance to *Botrytis cinerea* and ethylene responses. New Phytol 195:450–460. https://doi.org/10.1111/j.1469-8137.2012.04160.x

Zhou Y, Liu Y, Wang S et al (2017) Molecular cloning and characterization of galactinol synthases in *Camellia sinensis* with different responses to biotic and abiotic stressors. J Agric Food Chem 65:2751–2759. https://doi.org/10.1021/acs.jafc.7b00377